Exploring the laminar connectome

Ittai Shamir [a], Omri Tomer [b], Ronnie Krupnik [b], Yaniv Assaf [a,b]

[a] Department of Neurobiology, Faculty of Life Sciences, Tel Aviv University, Tel Aviv, Israel

[b] Sagol School of Neuroscience, Tel Aviv University, Tel Aviv, Israel

Abstract

The human connectome is the complete structural description of the network of connections and elements that form the 'wiring diagram' of the brain. Because of the current scarcity of information regarding laminar end points of white matter tracts inside cortical grey matter, tractography remains focused on cortical partitioning into regions, while ignoring radial partitioning into laminar components. To overcome this biased representation of the cortex as a single homogenous unit, we use a recent data-derived model of cortical laminar connectivity, which has been further explored and corroborated in the macaque brain by comparison to published studies. The model integrates multimodal MRI imaging datasets regarding both white matter connectivity and grey matter laminar composition into a laminar-level connectome. In this study we model the laminar connectome of healthy human brains (N=20) and explore them via a set of neurobiologically meaningful complex network measures. Our analysis demonstrates a subdivision of network hubs that appear in the standard connectome into each individual component of the laminar connectome, giving a fresh look into the role of laminar components in cortical connectivity and offering new prospects in the fields of both structural and functional connectivity.

Introduction

The human connectome is the comprehensive structural description of the network of connections and elements that form the human brain's 'wiring diagram'. The importance of exploring the connectome lies not only in uncovering patterns of structural connectivity across the brain, but also in understanding the functional states that emerge from it. For these reasons and more, uncovering the human connectome is a crucial and central mission in neuroscientific research (Sporns et al. 2005).

Since its foundation, the Human Connectome Project has lead the mission to map the connectome using non-invasive neuroimaging techniques, showcasing great progress particularly in MRI imaging of white matter connectivity (Van Essen et al. 2013, Setsompop et al. 2013). Concurrently to the progress in white matter imaging through MRI, promising strides are also being made in imaging of the laminar composition of cortical grey matter (Clark et al. 1992, Barbier et al. 2002, Duyn et al. 2007, Barazany and Assaf 2012, Glasser et al. 2014, Shafee et al. 2015, Lifshits et al. 2018, Shamir et al. 2019, Assaf 2019).

Despite growing progress in connectomics, starting from the macroscale and progressing gradually into higher resolutions in meso- and micro- scales, the field remains inherently limited by the biased representation of the cortex as a single homogenous unit. Due to the current scarcity of information regarding laminar end points of white matter tracts inside the cortical grey matter, tractography remains focused on transverse partitioning of the cortex into regions, while ignoring radial partitioning into laminar components (Jbabdi and Johansen-Berg 2011).

The integration of macrostructural data regarding white matter connectomics and microstructural data regarding grey matter laminar composition poses a promising development in the field of connectomics (Johansen-Berg 2013). A recently published study offers a simplified granularity-based model of cortical laminar connectivity based on published tract tracing and histological findings, with the purpose of integrating white and grey matter datasets derived from multimodal MRI imaging (Shamir and Assaf 2020a). The model is then further explored in the macaque brain and corroborated in its visual cortex by comparison to published studies (Shamir and Assaf 2020b). The resulting micro-level connectome offers a more detailed and unbiased representation of the connectome and offers new prospects in the field of both structural and functional connectivity on the laminar level.

In this study we model the laminar connectome of the healthy human brain (N=20 healthy subjects) and explore it via a set of neurobiologically meaningful complex network measures. We focus on investigating network hubs in the standard cortical connectome versus those in our modelled cortical laminar connectome.

Methods and materials

The framework for modelling cortical laminar connectivity (Shamir and Assaf 2020a) was applied on a set of 20 healthy human subjects.

Subjects

Twenty healthy human subjects (N=20), including 8 male and 12 female, 18-78 years old. Subjects were neurologically and radiologically healthy with no history of neurological diseases. The imaging protocol was approved by the institutional review boards of Sheba Medical Center and Tel Aviv University, where the MRI investigations were performed. All subjects signed informed consent before enrollment in the study.

Each subject was scanned on a 3T Magnetom Siemens Prisma (Siemens, Erlangen, Germany) scanner with a 64-channel RF coil. The sequences include:

1. A standard diffusion-weighted imaging (DWI) sequence, with the following parameters: Δ/δ=60/15.5 ms, b max=5000 (0 250 1000 3000 & 5000) s/mm2, with 87 gradient directions, FoV 204 mm, maxG= 7.2, TR=5200 ms, TE=118 ms, 1.5×1.5×1.5 mm^3, 128×128×94 voxels. This sequence was used to map the cortical connectome.
2. An MPRAGE sequence, with the following parameters: TR/TE = 1750/2.6 ms, TI = 900 ms, 1×1×1 mm^3, 224×224×160 voxels, each voxel fitted with a single T1 value.

3. An inversion recovery echo planar imaging (IR EPI) sequence, with the following parameters: TR/TE = 10,000/30 ms and 60 inversion times spread between 50 ms up to 3,000 ms, 3×3×3 mm^3, 68×68×42 voxels, each voxel fitted with up to 7 T1 values (Lifshits et al. 2018).
   These two sequences (2 and 3) were used to characterize the cortical layers.

Image processing

The following datasets were analyzed across Brainnetome atlas regions (see Supplementary Material Table 1), a connectivity-based parcellation which consists of 210 cortical regions and 36 subcortical subregions (Fan et al. 2016):

1. **Global white matter connectivity analysis**- each DWI dataset was analyzed for global white matter connectivity using MRtrix3 software package (Tournier et al. 2019). For a visualization of the resulting connectivity matrix of the 20-subject average, see figure 1A (below).

2. **Cortical laminar composition analysis**- each IR EPI dataset and its corresponding MPRAGE were analyzed for cortical laminar composition using our novel framework (Shamir et al. 2019). For a visualization of the resulting cortical laminar composition, averaged across all 20 subjects, see figure 1B (below).

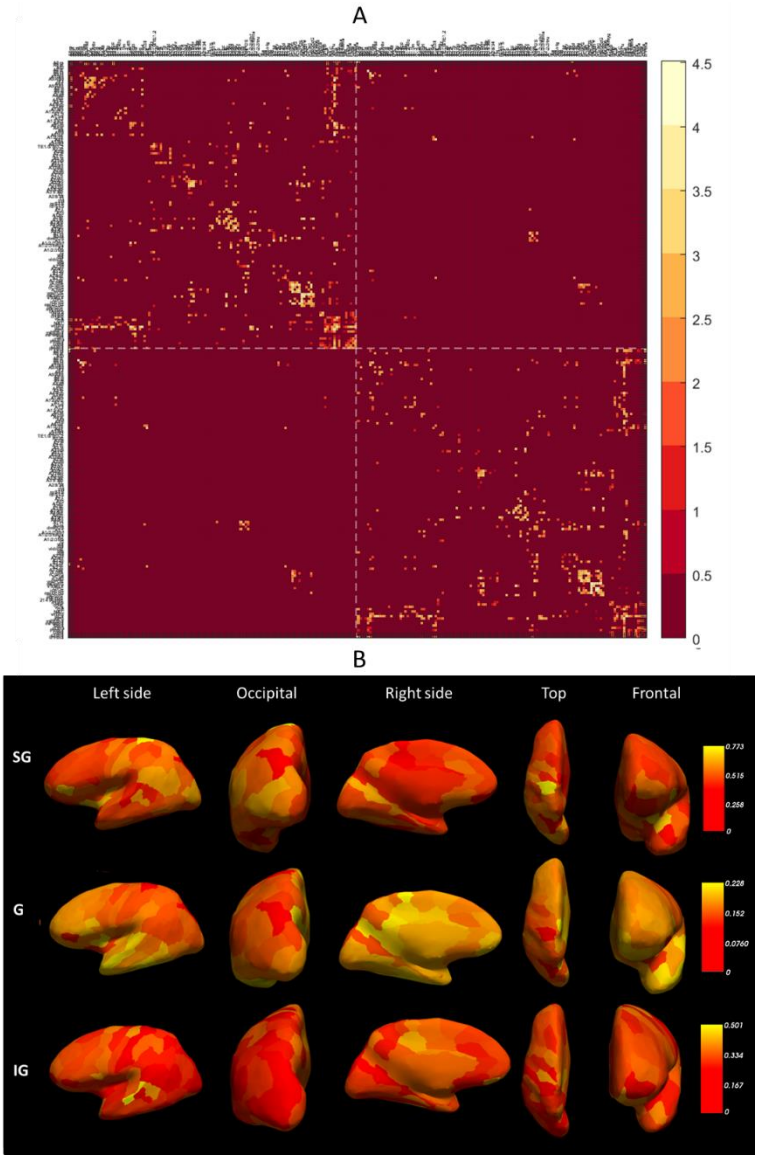

Fig. 1 Global white and gray matter datasets across Brainnetome atlas regions:

A- Average cortical connectivity (of all 20 subjects): average connectivity matrix, representing (log(number of tracts)) for connections that appear in at least 75% of subjects (color scheme adapted from Charles 2021)

B- Average cortical laminar composition (of all 20 subjects): where: top row- supragranular layers (SG), middle row- granular layer (G), bottom row- infragranular layers (IG), and columns represent different viewpoints

3. **Model of cortical laminar connectivity-** White and grey matter multimodal MRI datasets were integrated using our novel data-derived, granularity-based model of cortical laminar connectivity (Shamir and Assaf 2020a, 2020b). To implement our model in the Brainnetome atlas space, we labelled each region according to its granularity index (similarly to the labelling by Shamir and Assaf 2020a, see Supplementary Material figure 1). For a visualization of the 20-subject average of the resulting model of cortical laminar connectivity, see figure 2 (below).

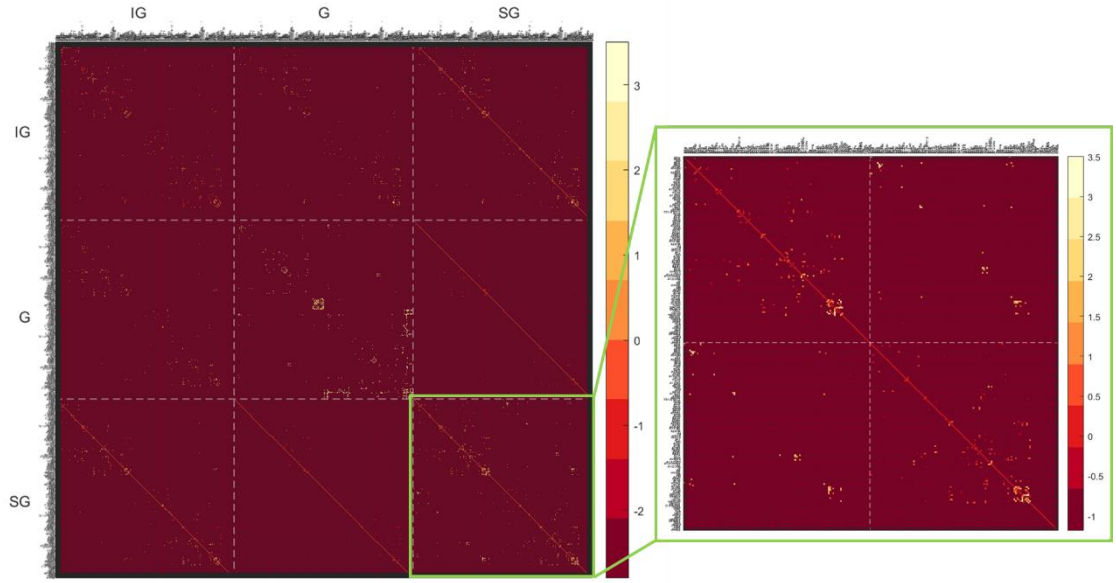

Fig. 2 Average cortical laminar connectivity (of all 20 subjects):
Average supra-adjacency matrix, representing whole-brain laminar-level connections across Brainnetome atlas regions, where the following abbreviations correspond to laminar components: IG- infragranular, G- granular, SG- supragranular. Model results are displayed as log(number of tracts) for all connections that appear in at least 75% of subjects (color scheme adapted from Charles 2021)

The variability of the resulting connectomes, representing both standard connectivity and laminar connectivity across subjects (N=20), are then evaluated. Subsequently, both connectomes are then explored via a set of neurobiologically meaningful complex network measures (Rubinov and Sporns 2010).

4. **Complex network analysis**

Once the standard connectome was extracted and the laminar connectome was modelled, we used tools for network analysis to explore their connectivity patterns and unique network features:

a. **Network complexity:** both connectomes were initially tested for non-trivial topological features that occur in complex networks, such as a heavy tail in degree distribution, but do not occur in simple networks, such as random graphs (see figure 3 below).

b. **Network analysis:** once the complexity of the both networks was shown, we explored and compared the average standard connectome to the components of the average laminar connectome. Global connectivity measures, including global efficiency and connectivity density, were chosen in order to evaluate the cost-efficiency trade-off. Additionally, a set of neurobiologically-meaningful local connectivity measures were calculated, including centrality measures (such as degree), as well as measures of integration (such as local efficiency) and segregation (such as clustering coefficient).

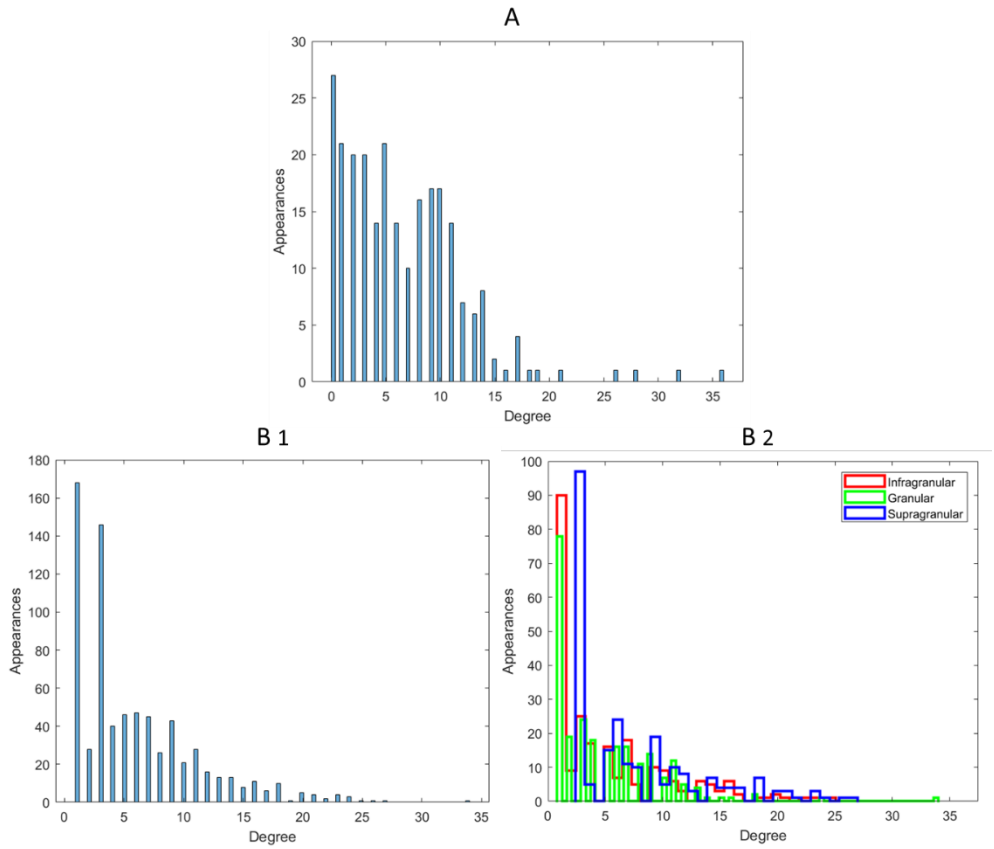

Fig. 3 Degree distributions:
Distributions of degrees for both the standard cortical connectome (A), as well as the cortical laminar connectome (B1), of the average connectomes for all connections that appear in at least 75% of subjects. For the laminar connectome, distributions for each laminar connectome are colored individually (B2): infragranular (IG)- red, granular (G)- green, supragranular (SG)- blue
Notice the positive skew, or "heavy-tail", in degree distributions in both cases and expressly in the laminar connectome

Results

After calculating average matrices for both standard cortical and cortical laminar connectomes, the variability of both connectomes was evaluated across all N=20 subjects (see figure 4). The standard connectome exhibits relatively higher standard deviation values, that correspond to the overall higher range of connectivity values. The subcorticocortical connections exhibit relatively higher standard deviation within each matrix, specifically in the granular to granular connections for the laminar connectome. This can be attributed to the higher connection values of subcorticocortical connections, relative to corticocortical connections.

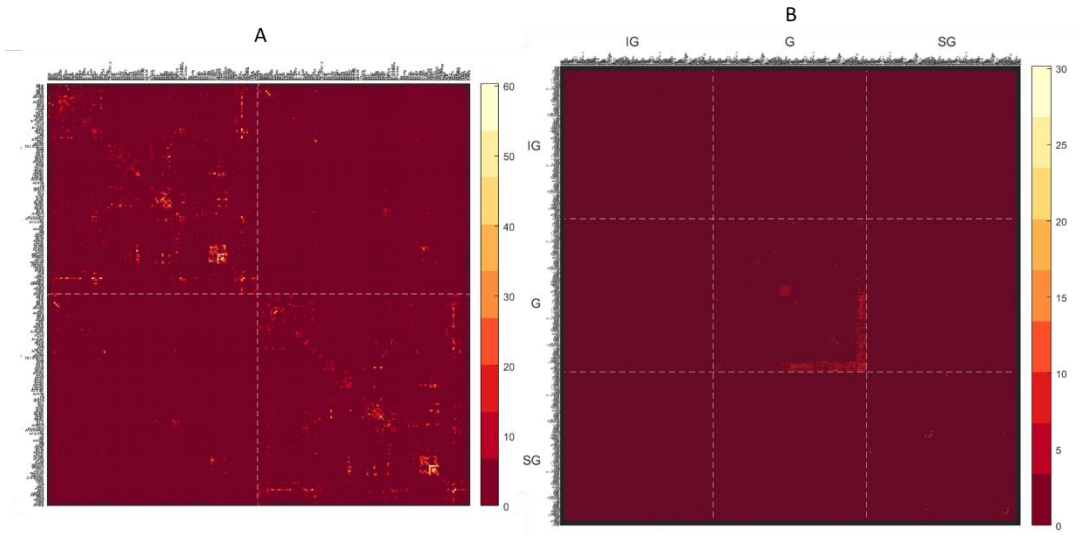

Fig. 4 Standard deviation of connectivity patterns of both connectomes (20 subjects):
A- Standard deviation of standard cortical connectivity across Brainnetome atlas regions
B- Standard deviation of cortical laminar connectivity across Brainnetome atlas regions (color scheme adapted from Charles 2021)

Two measures of global network connectivity were calculated for both the average standard and average laminar connectomes:

a. Global efficiency- an efficiency measure representing the average inverse shortest path length in the network.
b. Connection density- a cost measure representing the number of edges in a network as a proportion of the maximum possible number of edges.

The two measures where then plotted against one another to evaluate the cost-efficiency trade-off (Bullmore and Sporns 2012) in both connectomes (see figure 5).

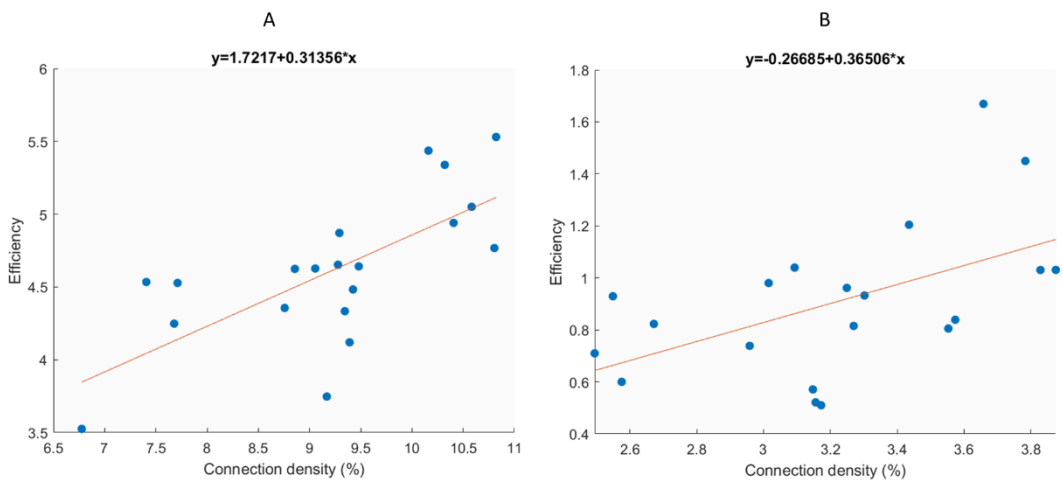

Fig. 5 Cost-efficiency trade-offs of both connectomes:
Global efficiency and connection density values, fitted to a linear regression model (top center), for all N=20 subjects, including the standard cortical connectomes (A) and the cortical laminar connectomes (B)

Examination of the cost-efficiency trade-off in the cortical laminar connectome shows that both the connection density as well as the global efficiency are reduced compared to the standard connectome. Connection density is a value inversely related to the maximum possible number of edges in the standard connectome: $Max_{edges\ standard} = \frac{N^2-N}{2}$, where N is the number of nodes in the standard connectome network. The number of nodes in the laminar connectome equals $3 * N$, since the cortex is divided into three cortical components. Accordingly, the maximum possible number of edges in the laminar connectome for big networks (large enough N): $Max_{edges\ laminar} \sim 9 * Max_{edges\ standard}$. Since the density is inversely related to the maximum possible number of edges, theoretically the ratio should be:

$Density_{laminar} \sim \frac{1}{9} * Density_{standard}$. In practice, the laminar connectome exhibits higher density than expected that instead follows: $Density_{laminar} \sim \frac{1}{3} * Density_{standard}$ (see density value range in figure 5). Global efficiency is a value inversely related to the mean shortest path (MSP), where: $MSP_{standard} \alpha N$. Since the laminar connectome has $3 * N$ nodes, the efficiency of the laminar connectome should follow: $Efficiency_{laminar} \sim \frac{1}{3} * Efficiency_{standard}$. In this case, the laminar connectome does approximately follow this ratio (see efficiency range in figure 5). Consequently, the efficiency to density ratio for the laminar connectome is slightly higher than for the standard connectome.

In order to examine the connectivity patterns of both the standard connectome as well as the cortical laminar connectome, we conducted an analysis of a selection of neurobiologically meaningful network measures (Rubinov and Sporns 2010). These measures include the following:

1. Degree- the number of edges connected to a node
2. Strength- sum of all neighboring edge weights (weighted degree)
3. Core/periphery- a partition of the network into two non-overlapping groups of nodes (core and periphery), maximizing within core edges and minimizing within periphery edges.
4. Clustering coefficient- the fraction of a node's neighbors that are also neighbors of each other
5. Local efficiency- the global efficiency (the average inverse shortest path length in the network) computed on node neighborhoods
6. Betweenness- the fraction of all shortest paths in the network that pass through a node

For a full visualization of the distribution of measure values across Brainnetome regions for the average connectomes, see figure 7 (below).

When examining the degree values across both connectomes, subcortical regions (thalamus, caudate, putamen and hippocampus) alongside a set of cortical regions appear as hubs with high degree values, including: superior frontal regions (A9m, A10m), superior parietal regions (A7 subregions), superior occipital regions (msOccG) and the cuneus (rCunG). These hubs exhibit high degree and strength in the standard connectome, as well as cumulatively across components of the laminar connectome. The infragranular and supragranular components do not include the subcortex but include cortical hubs, while the granular component includes the subcortex and mainly non-frontal hubs such superior parietal and superior occipital regions.

When examining the strength (weighted degree) values, a similar more generalized pattern appears. In the standard connectome, the subcortex overpowers the distribution across nodes and exhibits the highest strength values, followed by occipital and parietal regions. In the laminar connectome, the cortical regions appear once again in a cumulative fashion across components. The infragranular component exhibits symmetric bihemispheric strength distribution across all cortical regions, except the frontal cortex and the subcortex. The granular component includes high strength values in the subcortex and in medial regions of the frontal and parietal lobes. The supragranular component includes high strength values in occipital regions as well as frontal medial regions.

The distribution of degree and strength values in the standard connectome reestablish the notion of a rich-club bihemispheric organization that includes subcortical regions (van den Heuvel and Sporns 2011, 2013). The distribution of these values across components of the laminar connectome exhibit a cumulative nature, which is strengthened upon further examination of the core/periphery partitioning in the standard connectome. The standard connectome displays a core of highly interconnected hubs across the cortex and subcortex, a subset of these hubs appears in each individual component of the laminar connectome. The infragranular component displays hubs across non-frontal cortical regions, the granular component displays hubs that include subcortical regions, and the supragranular component displays hubs that include frontal cortical regions.

When examining the clustering coefficient and local efficiency in the standard connectome, temporal (A37), occipital (mOccG) and frontal (A44) regions exhibit high clustering and efficiency values. In comparison, across the laminar connectome the infra- and supragranular components exhibit a more even distribution across cortical regions, while the granular component exhibits high clustering and efficiency values in subcortical regions.

When examining the betweenness values in both connectomes, a relative hemispheric asymmetry appears in comparison to the measures discussed above. In the standard connectome, the subcortex exhibits high betweenness in regions such as the globus pallidus, hippocampus, thalamus, caudate and putamen.

Additionally, frontal medial and occipital regions exhibit some asymmetric betweenness values. The asymmetry is more pronounced in the laminar connectome, and specifically in the granular and supragranular components.

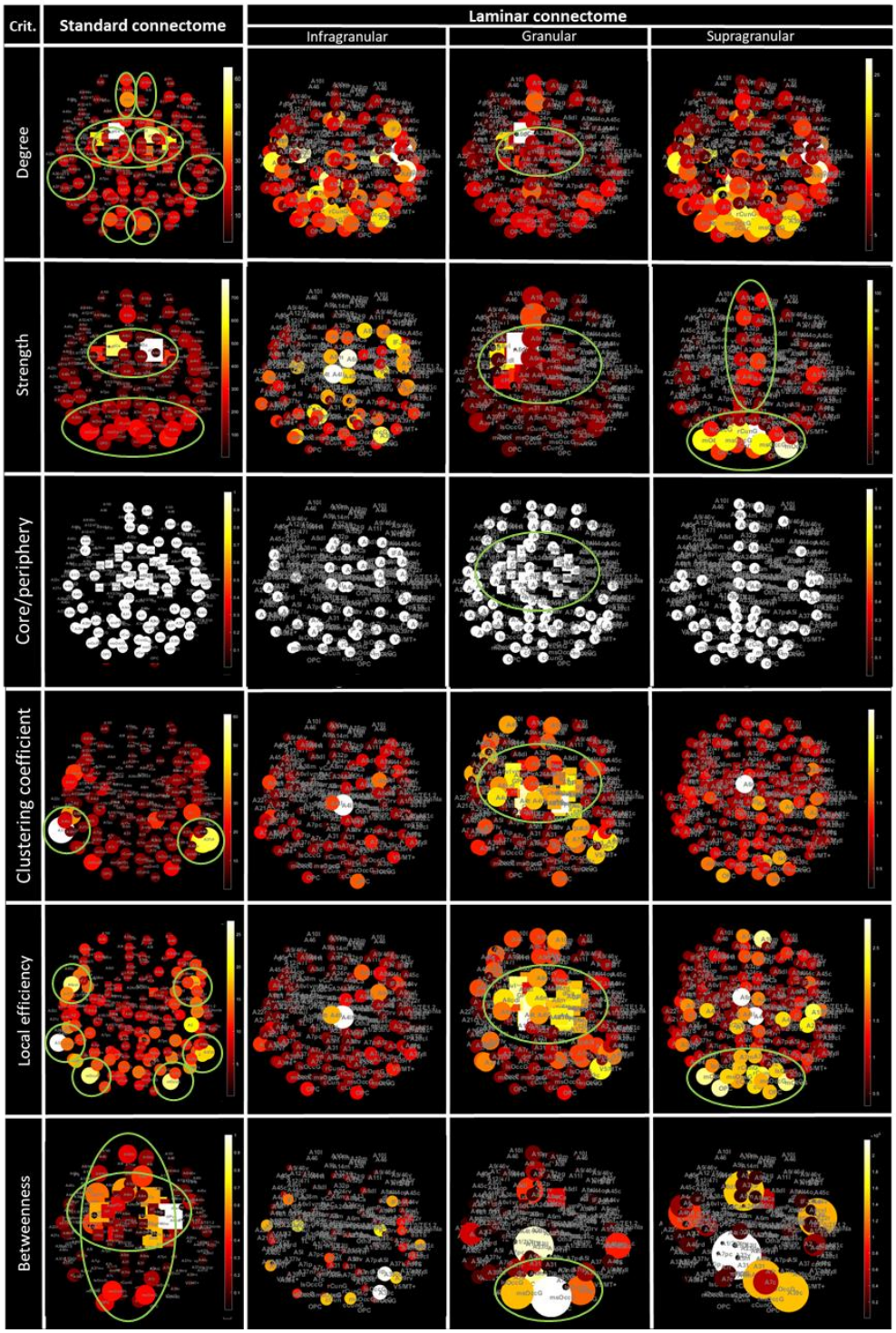

Fig. 6 Comparison of average connectomes:
Average standard connectome (left column) compared to components of the average laminar connectome (3 right columns, left to right: infragranular, granular and supragranular), where each row depicts a network measure (from top to bottom): degree, strength, clustering coefficient, local efficiency, betweenness and eigenvector. Cortical nodes represented as circles, and subcortical nodes as squares. Node color and size scaled according to network measure values. Noteworthy features circled in green

Discussion

In this study we model and explore the laminar connectome of N=20 healthy subjects using multimodal MRI imaging datasets. These datasets include both white matter connectivity and grey matter laminar composition, which are integrated using our novel model of cortical laminar connectivity (Shamir and Assaf 2020a, 2020b). The resulting laminar-level connectome is then explored across the Brainnetome atlas regions (Fan et al. 2016) using a set of neurobiologically meaningful complex network measures (Rubinov and Sporns 2010), while focusing on comparison of the cortical laminar connectome to standard cortical connectome.

When we examine both connectomes on a global scale, several similarities and several differences appear. On the similarity side, both connectomes exhibit a heavy tail in their degree distributions, which is even more noticeable in the laminar connectome. A heavy tail in a degree distribution is a non-trivial topological feature that occurs in complex networks but does not occur in simple or random networks. This feature is also associated with higher network resilience to nodal removal (regional damage). On the difference side, the standard connectome exhibits relatively higher standard deviation values across subjects, relative to the laminar connectome. This higher variability corresponds to the overall higher range of connectivity values in the standard connectome. Nonetheless, both connectomes exhibit higher variability in subcorticocortical connections, which can once again be attributed to stronger connections relative to corticortical connections. An additional difference between the two connectomes appears when exploring the cost-efficiency trade-offs, by plotting global efficiency against connection density. The laminar connectome exhibits higher connection density than expected based on the relative number of nodes in the network alone. With regards to efficiency, the laminar connectome exhibits a relatively lower global efficiency, as expected based on number of nodes alone. Nonetheless, the efficiency to density ratio is maintained and is even slightly higher for the laminar connectome relative to the standard connectome. This phenomenon may relate to the more refined definition of a node in the laminar network, where a node represents not only a regional location across the cortical surface, but also a laminar position in the vertical cross section of that location.

When we examine both connectomes on a local scale using complex network measures, we get a more nuanced image of connectivity patterns across the brain. With regards to measures of centrality, which represent the importance individual nodes, the following measures were chosen, including degree, strength, betweenness and core/periphery. When examining hemispheric symmetric, several dissimilarities appear across the examined centrality measures. While degree and strength value exhibit high hemispheric symmetry, core/periphery exhibits some hemispheric asymmetry and betweenness exhibits even higher asymmetry, particularly in components of the laminar connectome. On the other hand, several similar patterns appear across these four centrality measures. The first similarity involves high centrality of the subcortex in the standard cortical connectome, as well as in the granular component of the laminar connectome. The second similarity involves high centrality of occipitoparietal regions and low centrality of frontal regions in the infragranular component, particularly compared to the supragranular component.

With regards to measures of segregation, which represents specialized processing in clusters of nodes, and integration, which represents the network's ability to combine information, two measures were chosen. Clustering coefficient was chosen as a measure of network segregation, and local efficiency was chosen as a measure of network integration. With regards to dissimilarities between the measures, it appears that in the standard connectome the subcortex exhibits a low clustering coefficient and high local efficiency. The distribution of local efficiency values across the standard connectomes is more even, compared to higher clustering coefficient values specifically in frontal regions. Lastly, the network hubs are more pronounced for clustering coefficients in the laminar components, and more pronounced for local efficiency in the standard connectome. Nonetheless, several similar patterns appear across these two measures, primarily hemispheric symmetry in values and high values for subcortical regions in the supragranular component of the laminar connectome. Additionally, these measures exhibit several hubs in occipitotemporal regions.

From the exploration of network measures, and particularly from examining regions with high centrality values, several network hubs appear. In the standard cortical connectome, these hubs follow a similar pattern of previously discovered hubs that include the precuneus, superior frontal cortex and superior parietal cortex in both hemispheres, as well as subcortical regions (Van den Heuvel and Sporns 2013). Our findings show hubs across the Brainnetome atlas that include superior frontal regions (A10m, A9m),

superior parietal regions (A7 subregions), superior occipital regions (msOccG), the cuneus (rCunG), and subcortical regions (thalamus, caudate, putamen and hippocampus). In the cortical laminar connectome, these hubs appear selectively in specific laminar components: the infragranular component exhibits all hubs except frontal regions and the subcortex, the granular component exhibits hubs mainly in occipital and parietal regions as well as the subcortex, and the supragranular component exhibits most hubs, including frontal regions and excluding the subcortex. These findings are clearly summarized in the core/periphery partitioning of the standard connectome and its subdivision into components of the laminar connectome. In other words, the set of highly interconnected regions (hubs) that appear in the standard connectome also appear in the laminar connectome, with a specific subset of those hubs apparent within each laminar component.

This study presents an innovative exploration of a network model of the healthy human connectome on the laminar level. Due to the innovative in vivo nature of this model, corroborating the results in the human brain is a difficult task. Nonetheless, by using neurobiologically meaningful network measures, we see that the laminar-level connectome exhibits not only network complexity, but also a variety of repeated regional hubs. The components of the laminar connectome exhibit a symmetric cumulative nature in some features, while exhibiting an asymmetric noncumulative nature in others.

The characterization of the healthy human laminar connectome presented here could help in investigating pathologies that are assumed to involve abnormalities in layer-dependent cortical connectivity, such as schizophrenia and autism. Using complex network analysis tools such as the ones implemented here, the patterns of connectivity behind such conditions could be further examined and elucidated.

References:

1. Sporns O., Tononi G., Kotter R. (2005). *The Human Connectome: A Structural Description of the Human Brain*, PLoS Computational Biology 1(4): e42, 0245-0251. https://doi.org/10.1371/journal.pcbi.0010042
2. Van Essen D. C., Smith S. M., Barch D. M., Behrens T. E. J., Yacoub E., Ugurbil K.. (2013). *The WU-Minn Human Connectome Project: An Overview*, NeuroImage 80, 62-79. https://doi.org/10.1016/j.neuroimage.2013.05.041
3. Setsompop K., Kimmlingen R., Eberlein E., Witzel T., Cohen-Aded J., McNab J. A., Keil B., Tisdall M. D., Hoecht P., Dietz P., Cauley S.F., Tountcheva V., Matschl V., Lenz V. H., Heberlein K., Potthast A., Thein H., Van Horn J., Toga A., Schmitt F., Lehne D., Rosen B. R., Wedeen V., Wald L. L. (2013). *Pushing the limits of in vivo diffusion MRI for the Human Connectome Project*, NeuroImage. 80. 220-233. https://doi.org/10.1016/j.neuroimage.2013.05.078
4. Assaf Y., Bouznach A., Zomet O., Marom A., Yovel Y. (2020). *Conservation of brain connectivity and wiring across the mammalian class*, Nature Neuroscience, 23, 805–808. https://doi.org/10.1038/s41593-020-0641-7
5. Jbabdi S., Johansen-Berg J. (2011). *Tractography: Where Do We Go from Here?*, Brain Connectivity, Vol. 1, Num. 3, 169-183. https://doi.org/10.1089/brain.2011.0033
6. Johansen-Berg H. (2013). *Human connectomics – What will the future demand?*, NeuroImage, 80, 541-544. https://doi.org/10.1016/j.neuroimage.2013.05.082
7. Assaf Y., Johansen-Berg H., Thiebaut de Schotten M. (2019). *The role of diffusion MRI in neuroscience*. NMR in Biomedicine. 32:e3762. https://doi.org/10.1002/nbm.3762
8. Clark, V. P., Courchesne, E., & Grafe, M. (1992). *In vivo myeloarchitectonic analysis of human striate and extrastriate cortex using magnetic resonance imaging*. Cereb Cortex, 2, 417–424. https://doi.org/10.1093/cercor/2.5.417
9. Barbier E. L., Marrett S., Danek A., Vortmeyer A., van Gelderen P., Duyn J., Bandettini P., Grafman J., Koretsky A. P. (2002). *Imaging cortical anatomy by high-resolution MR at 3.0T: detection of the stripe of gennari in visual area 17*, Magnetic Resonance in Medicine, 48:735–738. https://doi.org/10.1002/mrm.10255
10. Duyn J. H., van Gelderen P., Li T. Q., de Zwart J. A., Koretsky A. P., Fukunaga M. (2007). *High-field MRI of brain cortical substructure based on signal phase*, PNAS, 104:28:11796–11801. https://doi.org/10.1073/pnas.0610821104

11. Glasser M. F., Goyal M. S., Preuss T. M., Raichle M. E., Van Essen D. C. (2014). *Trends and properties of human cerebral cortex: correlations with cortical myelin content*, NeuroImage, 93:165–175. https://doi.org/10.1016/j.neuroimage.2013.03.060
12. Shafee R., Buckner R. L., Fischl B. (2015). *Gray matter myelination of 1555 human brains using partial volume corrected MRI images*. NeuroImage, 105:473–485. https://doi.org/10.1016/j.neuroimage.2014.10.054
13. Barazany, D., & Assaf, Y. (2012). *Visualization of Cortical Lamination Patterns with Magnetic Resonance Imaging*. Cerebral Cortex, 22, 2016–2023. https://doi.org/10.1093/cercor/bhr277.
14. Lifshits, S., Tomer, O., Shamir, I., Barazany, D., Tsarfaty, G., Rosset, S., & Assaf, Y. (2018). *Resolution considerations in imaging of the cortical layers*. Neuroimage, 164, 112–120. https://doi.org/10.1016/j.neuroimage.2017.02.086
15. Assaf Y. (2019). *Imaging laminar structures in the gray matter with diffusion MRI*. Neuroimage. 197:677-688. https://doi.org/10.1016/j.neuroimage.2017.12.096
16. Shamir, I., Tomer, O., Baratz, Z., Tsarfaty, G., Faraggi,M., Horowitz, A., & Assaf, Y. (2019). *A framework for cortical laminar composition analysis using low-resolution T1 MRI images*, Brain Structure and Function, vol. 224, is. 4, 1457-1467. https://doi.org/10.1007/s00429-019-01848-2
17. Park H. J., Friston K. (2013). Structural and functional brain networks: from connections to cognition, Science, 342, 1238411. https://doi.org/10.1126/science.1238411
18. Shamir I., Assaf Y. (2020a). *An MRI-based, data-driven model of cortical laminar connectivity*, Neuroinformatics, (), 1-14. https://doi.org/10.1007/s12021-020-09491-7
19. Shamir I., Assaf Y. (2020b). *Modelling cortical laminar connectivity in the macaque brain*, bioRxiv preprint. https://doi.org/10.1101/2020.07.19.210526
20. Rubinov M., Sporns O. (2010). Complex network measures of brain connectivity: Uses and interpretations, NeuroImage, 52(3): 1059-1069. https://doi.org/10.1016/j.neuroimage.2009.10.003.
21. Fan L., Li H., Zhuo J., Zhang Y., Wang J., Chen L., Yang Z., Chu C., Xie S., Laird A. R., Fox P. T., Eickhoff S. B., Yu C., Jiang T. (2016). The Human Brainnetome Atlas: A New Brain Atlas Based on Connectional Architecture. Cerebral Cortex, 26-8, 3508–3526. https://doi.org/10.1093/cercor/bhw157
22. Van den Heuvel M. P., Sporns O. (2011). *Rich-club Organization of the Human Connectome*, Journal of Neuroscience, 31(44), 15775-15786. https://doi.org/10.1523/JNEUROSCI.3539-11.2011
23. Van den Heuvel M. P., Sporns O. (2013). *Network hubs in the human brain*, Trends in Cognitive Sciences, 17(12), 683:696. https://doi.org/10.1016/j.tics.2013.09.012
24. Tournier JD, Smith RE, Raffelt D, Tabbara R, Dhollander T, Pietsch M, Christiaens D, Jeurissen B, Yeh C H, Connelly A. MRtrix3: A fast, flexible and open software framework for medical image processing and visualization. NeuroImage. 2019, 202, 116–37. https://doi.org/10.1016/j.neuroimage.2019.116137
25. Bullmore E, Sporns O (2012). The economy of brain network organization, Nature Reviews Neuroscience, 13(5), 336-49. https://doi.org/10.1038/nrn3214
26. Charles (2021). cbrewer: colorbrewer schemes for Matlab (https://www.mathworks.com/matlabcentral/fileexchange/34087-cbrewer-colorbrewer-schemes-for-matlab), MATLAB Central File Exchange. Retrieved March 15, 2021.